Polymerized Small Molecular Acceptor with Branched Side Chains for All Polymer Solar Cells with Efficiency over 16.7%

Yun Li, Jiali Song, Yicai Dong, Hui Jin, Jingming Xin, Shijie Wang, Yunhao Cai, Lang Jiang, Wei Ma, Zheng Tang, and Yanming Sun**

Y. Li, J. Song, Dr. Y. Cai, Prof. Y. Sun

School of Chemistry

Beihang University

Beijing 100191, P. R. China

E-mail: caiyunhao@buaa.edu.cn; sunym@buaa.edu.cn

Y. Dong, Prof. L. Jiang

Key Laboratory of Organic Solids,

Institute of Chemistry,

Chinese Academy of Sciences,

Beijing 100190, P. R. China

H. Jin, Prof. Z. Tang

State Key Laboratory for Modification of Chemical Fibers and Polymer Materials, Center for Advanced Low-dimension Materials,

College of Materials Science and Engineering,

Donghua University

Shanghai, 201620, P. R. China

J. Xin, S. Wang, Prof. W. Ma

State Key Laboratory for Mechanical Behavior of Materials,

Xi'an Jiaotong University,

Xi'an 710049, P. R. China.

Abstract

The power conversion efficiencies (PCEs) of small molecule acceptor (SMA)-based organic solar cells have already exceeded 18%. However, the development of polymer acceptors still lags far behind their SMA counterparts mainly due to the lack of efficient polymer acceptors. Herein, we designed and synthesized a series of polymer acceptors named PY-X (with X being the branched alkyl chain) by employing the same central core with the SMA L8-BO but with different branched alkyl chains on the pyrrole motif. L8-BO with the branched alkyl chains on the beta position of the

thiophene unit has previously shown improved structural order and charge transport compared to those of Y6. It was found that the molecular packing of SMA-HD featuring 2-hexyldecyl side chain used in the synthesis of PY-HD is similar to L8-BO, in which the branched alkyl chains lead to condensed and high-order molecular assembly in SMA-HD molecules. When combined with PM6, PY-HD-based all polymer solar cell (all-PSC) exhibits a high PCE of 16.41%, representing the highest PCE value for the binary all-PSCs. Moreover, the side-chain modification on the pyrrole site position further improves the performance of the all-PSCs, and the PY-DT-based device delivers a new record high efficiency of 16.76% (certified as 16.3%), with a high open-circuit voltage of 0.949 V, a short-circuit current of 23.73 mA cm^{-2} and a decent fill factor of 74.4%. Our work provides new insights for understanding the structure-property relationship of polymer acceptors and paves a feasible avenue to develop efficient conjugated polymer acceptors.

1. Introduction

In the past decade, polymer solar cells (PSCs) have witnessed significant progress due to the rapid development of small molecule acceptors (SMAs), and the power conversion

efficiencies (PCEs) of state-of-the-art PSCs have surpassed 18%.[1-7] Compared to the SMA-based PSCs, all polymer solar cells (all-PSCs), consisting of two conjugated polymers as both electron donor and electron acceptor, have more notable merits of excellent mechanical robustness, morphological stability, and suitable for flexible device fabrication.[8-11] Despite the numerous advantages of all-PSCs, much less attention has been devoted to all-PSCs, and only a few all-PSCs can yield PCEs over 15%,[12-14] which lags far behind the SMA-based PSCs. To boost the PCEs of all-PSCs, one of the most effective approaches is developing novel polymer acceptors.

In the early stage of all-PSCs, polymer acceptors were mainly constructed with building blocks such as perylene diimide,[15-16] naphthalene diimide,[17] and boron-nitrogen coordination units,[18] *etc*. Unfortunately, naphthalene/perylene diimide polymer acceptors typically exhibit quite low extinction coefficient and strong crystallization tendency. B←N-bridged bipyridine-based polymer acceptors suffer from narrow absorption band and low electron mobility. In most cases, all-PSCs based on these kinds of polymer acceptors show PCEs < 10%.[19-21] Until 2017, Li *et al.* put forward a facile strategy of polymerizing SMAs into polymer acceptors (PSMAs).[22] PSMAs not only inherit the advantages of the SMAs, such as wide-range absorption,[23-24] easy tunability of the energy level and bandgap,[25-28] but also preserve the good film-forming capacity and morphological stability of the polymers.[29-30] More importantly, physicochemical and photovoltaic properties of the

PSMAs can be fine-tuned by copolymerizing appropriate SMA building blocks with different aromatic units.[31-35] Afterwards, a series of PSMAs were designed and synthesized. Among them, Y6-series SMA-based PSMAs exhibit obviously improved photovoltaic performance,[36-39] narrowing the efficiency gap with SMA-based PSCs. Since SMA serves as the main building block of conjugated polymer acceptor, its property especially the molecular packing and charge transport behaviour could strongly influence the performance of the resultant polymer.[40] From this perspective, systematic investigations on the relationships between SMA's structures and the properties of PSMAs are urgently needed, which can aid in better design of new PSMAs for further improving the PCEs of all-PSCs.

In our previous work, we reported a highly efficient SMA named L8-BO by substituting the beta position of the thiophene unit on a Y6-based dithienothiophen[3,2-b]-pyrrolobenzothiadiazole core with branched alkyl chains.[41] It was revealed that the branched alkyl chain modification could utterly change the molecular packing behavior of L8-BO, leading to improved structural order and charge transport in thin film and thereby an unprecedented efficiency of 18.32% with a high fill factor (FF) of 81.5% was achieved. Inspired by the success of L8-BO, we further extend this approach into the design of PSMAs. Herein, a series of PSMAs, PY-X (with X being the branched alkyl chain), were synthesized by employing L8-BO's core as the main building block, and different branched alkyl chains attached on the pyrrole motif. Precise molecular packing was

investigated in single crystals. It was found that the molecular packing of SMA-HD (2-hexyldecyl substitution) used in the synthesis of PY-HD is similar to that of L8-BO, in which the branched alkyl chains lead to a more condensed molecular assembly in SMA-HD molecules compared to Y6 (Figure 1).[42] When polymerized with thiophene unit, the PY-HD shows a high electron mobility of 7.76×10^{-4} cm^2 V^{-1} s^{-1}. After blended with PM6, PY-HD-based all-PSC yields a high PCE of 16.41%, representing the highest efficiency reported for binary all-PSCs thus far. Moreover, after subtle side chain modification of SMA-DT on the pyrrole motif to tune the energy level, molecular packing, and miscibility with the PM6, PY-DT (2-decyltetradecyl substitution)-based all-PSC affords a new record high PCE of 16.76%, with an extremely low non-radiative voltage loss of 0.18 V and a high open-circuit voltage (V_{oc}) of 0.949 V. Additionally, these all-PSCs exhibit excellent photostability under continuous illumination. Our work indicates that by judiciously optimizing the SMA building block of PSMAs, the PCE of all-PSC can be effectively improved.

2. Results and Discussion

The molecular structures and synthetic routes of the PY-X are shown in Scheme 1. The synthetic procedures are described in the Supporting Information. The target monomers of SMA-X were characterized by ^{1}H nuclear magnetic resonance (NMR) and mass spectra (MALDI-TOF) (Figure S1-S8). The target polymers of PY-X were synthesized via the Stille

polycondensation of SMA-X and 2,5-bis(trimethylstannanyl) thiophene. As measured by gel permeation chromatography using 1,2,4-trichlorobenzene as the eluent at 150 ^{o}C (Figure S9), the PY-X acceptors display the number-average molecular weights (M_n)/polydispersity index with 7.6 kDa/2.35, 8.6 kDa/1.91, 7.2 kDa/1.98, and 9.2 kDa/1.88 for PY-HD, PY-OD (2-octyldodecyl substitution), PY-DT, and PY-DH (2-dodecylhexadecyl substitution), respectively. All the PY-X acceptors can be well dissolved in chloroform, chlorobenzene and toluene. Thermogravimetric analysis (TGA) was performed to measure the thermal stabilities of these acceptors, and all the PY-X acceptors exhibit similar decomposition temperatures of around 370 ^{o}C with 5% weight loss under nitrogen atmosphere, indicating the excellent thermal stability of these materials (Figure S10).

The chemical structures of Y6, L8-BO and SMA-HD are shown in Figure 1a. In our previous work, we showed that although Y6 and L8-BO share the same dithienothiophen[3,2-b]-pyrrolobenzothiadiazole core, the introduction of 2-butyloctyl in L8-BO rather than the linear alkyl chain in Y6 on the beta position of the thiophene unit can completely change the molecular packing symmetry, which leads to a more condensed and high-order molecular assembly in L8-BO.[16,17] Similarly, SMA-HD also possesses the 2-butyloctyl on the beta position of the thiophene unit and 2-hexyldecyl side chain has been introduced on the pyrrole motif to enhance the molecular solubility. The single crystal of SMA-HD has been grown to investigate the molecular packing behaviour (Table S1). As

presented in Figure 1b, from the main view of the molecular conformation, the branched 2-butyloctyl chain in L8-BO and SMA-HD show shorter side-chain self-assembly distances than the linear hendecyl chain in Y6. From the side view of molecular conformations (Figure 1c), 2-butyloctyl chain in L8-BO and SMA-HD tilts out of the conjugated plane with shorter vertical distance compared to Y6, which is favorable of close π-π stacking of adjacent molecules. As a result, the average π-π distances are determined to be 3.258 Å, 2.834 Å, and 2.996 Å for Y6, L8-BO and SMA-HD, respectively (Figure S11 and Table S2). Overall, SMA-HD shows similar molecular packing with L8-BO and forms a molecular arrangement with small ellipse-shaped voids from a tilted c-axis projection, which is different from the Y6 packing that forms orthorhombic vacancies in the c-axis projection. From Figure 1d, it can be seen that compared to Y6, SMA-HD shows reduced marked lateral distances with a more condensed molecular assembly. The packing coefficients for Y6, L8-BO and SMA-HD were calculated to be 54.5%, 64.1% and 60.8%, respectively. Thus, the more condensed molecular assembly and closer π-π stacking in SMA-HD can facilitate charge transport and a high electron mobility in the corresponding PY-HD acceptor is anticipated.

The UV-vis absorption spectra of the PY-X acceptors were measured in both dilute solutions and thin films. In dilute chloroform solution (Figure S12a), PY-HD, PY-OD, and PY-DT exhibit similar maximum absorption peaks at 788 nm, while PY-DH shows obviously blue-shifted absorption with the main peak centered at 766 nm. As plotted in Figure 2a,

similar trend was observed in thin films. The main absorption peaks are concentrated at 812 nm for PY-HD, PY-OD, and PY-DT films, and 803 nm for PY-DH film. In comparison with the absorption in solutions, the red-shifted absorption spectra for PY-X films indicate more intimate π-π stacking interaction and aggregation in the solid state. With the increase of branched alkyl chain, the extinction coefficient of PY-HD to PY-DH slightly decreases from 0.68×10^5 to 0.54×10^5 cm^{-1} (Figure S12b). The absorption spectra of PY-X acceptors are well complemented to the polymer donor PM6, and their blends can almost cover the solar spectrum in the wavelength range of 300-900 nm (Figure S12c), ensuring decent photocurrent generations in the corresponding devices. The temperature dependence of absorption spectra of PY-X acceptors were further measured in the temperature range of 30-110 °C (Figure S13). All the PY-X acceptors in chlorobenzene show gradually decreased absorption peak intensity when temperature increases from 30 to 110 ^oC. It was found that the absorption peak and onset of PY-X acceptors in high-temperature solution are almost unchanged, suggesting their strong intermolecular interaction and π-π stacking. The electrochemical properties of PM6 and PY-X were studied by cyclic voltammetry measurements (Figure S14). The energy level diagrams of PM6 and PY-X are displayed in Figure 2b. The highest occupied molecular orbital (HOMO) and lowest unoccupied molecular orbital (LUMO) energy levels are estimated to be -5.52/-3.94, -5.60/-3.84, -5.60/-3.83, and -5.65/-3.76 eV for PY-HD, PY-OD, PY-DT, and PY-DH, respectively. It can

be seen that increasing the branched alky chain leads to up-shifted LUMO energy level, which is beneficial to a high V_{oc} in the related devices.

All-PSCs were fabricated to evaluate the photovoltaic performance of the PY-X acceptors. A conventional device architecture of indium tin oxide (ITO)/poly(3,4-ethylenedioxythiophene):polystyrene sulfonate (PEDOT:PSS)/active-layer/PNDIT-F3N/Ag has been used in this work. Figure 2c presents the current density versus voltage (*J-V*) curves of the PM6:PY-X devices, and Table 1 summarizes the photovoltaic parameters of the optimized devices. It is interesting to find that all-PSC based on PM6:PY-HD shows a high PCE of 16.41%, with a V_{oc} of 0.937 V, a J_{sc} of 24.05 mA cm^{-2} and an FF of 72.8%, representing the best PCE for the binary all-PSCs until now. Upon subtle side chain modification on the pyrrole motif, PY-OD-based all-PSC exhibits an improved PCE of 16.53%, with increased V_{oc} and FF. Further increasing the side chain to 2-decyltetradecyl leads to continuous improvement in photovoltaic performance and the best-performing all-PSC based on PM6:PY-DT produces a new record high PCE of 16.76% (certified as 16.3% in the National Institute of Metrology in China, Figure S15), with a high V_{oc} of 0.949 V, a J_{sc} of 23.73 mA cm^{-2} and an FF 74.4% (Figure 2d and Table S3). In contrast, despite the higher V_{oc} of 0.961 V, PY-DH-based all-PSC shows decreased J_{sc} and FF values, generating relatively lower PCE of 14.86%. The long branched side chain of 2-dodecylhexadecyl may influence the molecular packing and reduce π-π stacking

interactions, which contributes to the inferior performance achieved in PY-DH devices. The detailed results about the device optimization are collected in Figure S16-S19 and Tables S4-S7. Figure S20 exhibits the efficiency histograms of the all-PSCs. The counts versus PCE plot following Gaussian distributions for all devices supports that all-PSCs have reproducible PCEs with small deviations. In addition, we found that PY-DT shows good synthetic reproducibility. We synthesized five PY-DT batches under identical polymerization conditions. There is not serious batch-to-batch variation among these polymers, demonstrating the great potential for commercial-scale production of PY-DT. The detailed photovoltaic parameters of different PY-DT batches are presented in Table S8.

External quantum efficiency (EQE) spectra of all-PSCs are shown in Figure 2e. The PY-HD, PY-OD, and PY-DT-based devices show similar EQE spectra, with the maximum EQE response approaching 85% in the wavelength range of 430-630 nm, while the PY-DH-based device exhibits blue-shifted EQE spectra and the highest EQE response is about 74%, indicating reduced photon-to-electron conversion efficiency in this device. The integrated J_{sc}s calculated from the EQE spectra are 23.45, 23.30, 23.20, and 20.87 mA cm^{-2}, for PY-HD, PY-OD, PY-DT, and PY-DH based devices, respectively, which are well consistent with the values obtained from the *J-V* curves.

Apart from the photovoltaic performance, the stability is also vitally important for the practical application of all PSCs. We monitored the photostability of this series of all-PSCs

accordingly. As shown in Figure 2f, PM6:PY-HD, PM6:PY-OD, PM6:PY-DT, and PM6:PY-DH devices reached their T_{80} (the time required to reach 80% of initial performance) at 207, 245, 269, and 309 h, respectively, under continuous illumination. It is worthy mentioned here, the impressively high photostabilies of PM6:PY-DT and PM6:PY-DH devices are among the best results reported for all-PSCs. These promising results suggest that our molecular design approach can enable high efficiency and good photostability in the meantime, which is highly desirable for the large-scale fabrication of all-PSCs.

To clarify the influence of branched side chains on charge transport properties, the hole mobility (μ_h) and electron mobility (μ_e) of the pristine and blend films were calculated by using space-charge limited current (SCLC) method (Figure S21 and Table S9). The calculated μ_e mobilities of the neat PY-X acceptors are 7.76, 5.92, 5.47, and 2.54×10^{-4} cm^2 V^{-1} s^{-1} for PY-HD, PY-OD, PY-DT, and PY-DH, respectively. It can be seen that the increase of the branched side chains leads to decreased electron mobilities. As for the blend films, the μ_h and μ_e also decreases gradually from PM6:PY-HD to PM6:PY-DH. Notably, PM6:PY-DT device demonstrates a lowest μ_h/μ_e of 1.24. The more balanced charge transport of this combination contributes to its best photovoltaic performance achieved in the PM6:PY-DT device. In addition, PM6:PY-DH device affords a high μ_h/μ_e of 2.27, and the unbalanced

hole mobility and electron mobility in this system is considered as an important reason for the low PCE.

To probe the charge recombination behavior in the devices, the dependence of V_{oc} on the light intensity (P_{light}) was examined (Figure S22a). When the slope of V_{oc} versus the natural logarithm of P_{light} is equal to kT/q (where k is the Boltzmann constant, T is the Kelvin temperature and q is the elementary charge), bimolecular recombination is the dominant recombination mechanism. When the main recombination mechanism is trap-assisted recombination, a higher dependence of the V_{oc} on the light intensity ($>kT/q$) can be obtained.[43] Here, the slope values from the PY-HD to PY-DH are determined to be 1.33, 1.28, 1.23, and 1.40 kT/q, respectively. The smaller slope observed in PM6:PY-DT device indicates that the trap-assisted recombination is effectively suppressed inside the device, which contributes to the enhanced FF and PCE. Furthermore, the charge generation and exciton dissociation behaviour of these all-PSCs were studied by measuring the dependence of the photocurrent density (J_{ph}) on the effective voltage (V_{eff}) (Figure S22b).[44] The exciton dissociation probability (P_{diss}), determined from J_{ph} under the short-circuit condition divided by the saturated photocurrent density (J_{sat}), are 96.35%, 97.20%, 98.05%, and 96.32% for PM6:PY-HD, PM6:PY-OD, PM6:PY-DT, and PM6:PY-DH blends, respectively, indicative of the efficient charge generation and exciton dissociation in these devices, especially for the PM6:PY-DT device.

The morphology of the blend films was investigated by atomic force microscopy (AFM) and grazing incidence wide-angle X-ray scattering (GIWAXS). As shown in Figure 3a-d, clear fibrillar morphology can be seen for all the blend films with similar root-mean-square (RMS) values. Such morphology is beneficial for efficient exciton dissociation and charge transport (Figure S23).[45-46] The phase separation is strongly correlated with the miscibility of the donor and acceptor materials, which is investigated by calculating the Flory-Huggins interaction parameter χ. The contact angles of water and glycerol on neat PM6, PY-HD, PY-OD, PY-DT, and PY-DH films were measured (Figure S24). The surface tension (γ) can be calculated by using Wu's model[47] and the γ values are 20.3, 25.6, 22.37, 28.7, and 28.3 for PM6, PY-HD, PY-OD, PY-DT, and PY-DH, respectively(Table S10). Then the miscibility between the donor and acceptor can be calculated using the following empirical equation: $\chi \propto (\sqrt{\gamma_A} - \sqrt{\gamma_B})^2$.[48] The calculated χ values are 0.302, 0.723, 0.436 and 0.640 for PM6/PY-HD, PM6/PY-OD, PM6/PY-DT, and PM6/PY-DH. Such results suggesting a favorable phase separation with well defined fibrillar morphology in PM6:PY-DT blend, which contributes to its high performance as well.

The 2D GIWAXS pattern of the blend films are shown in Figure S25, and the corresponding line-cut intensities taken along the in-plane (IP) and out-of-plane (OOP) directions are shown in Figure 4f. All these blend films adopt preferred face-on orientations, evidenced by the strong (010) diffraction peaks in the OOP and lamellar (100) stacking peaks in the IP

direction. The crystalline correlation lengths (CCLs) for the lamellar and π-π stacking peaks in the blends are quantitatively calculated and the corresponding results are summarized in Table S11. The CCLs associated with the π-π stacking peaks are calculated to be 21.9 Å, 20.7 Å, 20.6 Å, and 19.0 Å for PM6:PY-HD, PM6:PY-OD, PM6:PY-DT, and PM6:PY-DH, respectively, indicating that the degree of molecular packing in the blends gradually decreases. The results agrees well with the SCLC mobility trend and also elucidates the performance differences in the corresponding all-PSCs.

It has been shown earlier that these polymer acceptors show similar absorption profile. However, the V_{oc} increases with the increasing size of the branched side chains for the PY-X-based all-PSCs. The origin of the high V_{oc}s together with the energy loss (E_{loss}) of these all-PSCs have been systematically investigated. The optical bandgap (E_{gap}) of the blend films were determined from the crossing point between optical absorption and photoluminescence (PL) spectra of active layers (Figure S26). The PM6:PY-HD, PM6:PY-OD, and PM6:PY-DT blends have the identical E_{gap} of 1.48 eV, whereas the PM6:PY-DH blend shows a slightly larger E_{gap} of 1.49 eV. The total energy loss can be calculated following the equation $E_{loss} = E_{gap} - qV_{oc}$. The E_{loss} values are determined to be 0.55, 0.55, 0.54, and 0.53 V for PM6:PY-HD, PM6:PY-OD, PM6:PY-DT, and PM6:PY-DH devices, respectively (Table 2). According to the detailed balance thoery,[49] the E_{loss} could be divided into three parts ($E_{loss} = \Delta E_1 + \Delta E_2 + \Delta E_3$). The first part ($\Delta E_1 = E_{gap} - qV_{oc}^{SQ}$) is defined as the difference between E_{gap}

and the upper limit for the open-circuit voltage derived in the Shockley-Queisser (SQ) theory (V_{oc}^{SQ}). This energy loss term is caused by the radiative recombination loss above the bandgap. For all the types of solar cells, the ΔE_1 is unavoidable. The V_{oc}^{SQ} value for PM6:PY-HD device is 1.21 V, and for the other three systems are 1.22 V. Therefore, the ΔE_1 values for these all-PSCs are calculated to be 0.27 V. The second part ($\Delta E_2 = qV_{oc}^{SQ} - qV_{oc}^{rad}$) mainly comes from the radiative recombination loss below the bandgap, and the ΔE_2 values for PM6:PY-HD, PM6:PY-OD, and PM6:PY-DT devices are 0.09 V, and for the PM6:PY-DH device is 0.08 V. The third part ΔE_3 is the non-radiative recombination loss, which can be calculated by the following equation: $\Delta E_3 = \frac{-kt}{q}\ln(EQE_{EL})$ (Figure S27).[50] This part of voltage loss is the main cause of the large voltage loss in organic solar cells. Encouragingly, the ΔE_3 values for the PY-HD, PY-OD, PY-DT and PY-DH-based all-PSCs are 0.19, 0.18, 0.18 and 0.18 eV, respectively. To the best of our knowledge, the ΔE_3 of 0.18 eV is the lowest non-radiative recombination loss value reported for all-PSCs (Figure S28), which is comparable to that (0.18 eV) of crystalline silicon solar cells. The results suggest that non-radiative recombination losses were effectively suppressed in the PY-X-based all-PSCs and help explain the reason for the high V_{oc}s achieved in these devices.

3. Conclusion

In conclusion, we developed a series of efficient polymer acceptors named PY-X. The PY-X acceptors were synthesized by adopting the L8-BO's framework as the main building block and introducing different branched side chains on the pyrrole unit. Single crystal reveals that the SMA-HD monomer has a more condensed molecular assembly and improved molecular order in comparison with Y6, which can facilitate charge transport in thin film. By polymerizing the SMA-HD with the thiophene unit, the resulting PY-HD-based all-PSC yields a high PCE of 16.41%. Moreover, upon using the side chain modification strategy, a champion efficiency of 16.76% associated with a V_{oc} of 0.949 V, a J_{sc} 23.73 mA cm^{-2} and an FF of 74.4% is recorded in PM6:PY-DT device. The improved efficiency in PM6:PY-DT device is mainly ascribed to the optimized phase separation with well-defined fibrillar morphology, balanced charge transport and suppressed non-radiative recombination. In addition, these all-PSCs show superior photostability under continuous illumination. Our results highlight the potential of PY-X in the fabrication of high-efficiency all-PSCs and also unveil the importance of SMA building block's optimization in constructing efficient conjugated polymer acceptors.

Supporting Information

Supporting Information is available from the Wiley Online Library or from the author

Acknowledgements

This work was financially supported by the National Natural Science Foundation of China (Grant No. 51825301, 21734001, and 52003013), and China Postdoctoral Science Foundation (BX20190023). X-ray data were acquired at beamline 7.3.3 at the Advanced Light Source, Lawrence Berkeley National Laboratory, which is supported by the Director, Office of Science, Office of Basic Energy Sciences, of the US Department of Energy under contract no. DE-AC02-05CH11231. The authors thank Chenhui Zhu at beamline 7.3.3, and Cheng Wang at beamline 11.0.1.2 for assistance with data acquisition.

Conflict of Interest

The authors declare no conflict of interest.

References

[1] M. Zhang, L. Zhu, G. Zhou, T. Hao, C. Qiu, Z. Zhao, Q. Hu, B. W. Larson, H. Zhu, Z. Ma, Z. Tang, W. Feng, Y. Zhang, T. P. Russell, F. Liu, *Nat. Commun.* **2021**, *12*, 309.

[2] Y. Li, Y. Cai, Y. Xie, J. Song, H. Wu, Z. Tang, J. Zhang, F. Huang, Y. Sun, *Energy Environ. Sci.* **2021**, *14*, 5009.

[3] Y. Cai, Y. Li, R. Wang, H. Wu, Z. Chen, J. Zhang, Z. Ma, X. Hao, Y. Zhao, C. Zhang, F. Huang, Y. Sun, *Adv. Mater.* **2021**, *33*, 2101733.

[4] L. Zhan, S. Li, X. Xia, Y. Li, X. Lu, L. Zuo, M. Shi, H. Chen, *Adv. Mater.* **2021**, *33*, 2007231

[5] Y. Xie, H. S.Ryu, L. Han, Y. Cai, X. Duan, D.Wei, H. Y. Woo, Y. Sun, *Sci. China Chem.* **2021**, *64*, 228.

[6] G. Liu, R. Xia, Q. Huang, K. Zhang, Z. Hu, T. Jia, X. Liu, H.-L. Yip, F. Huang, *Adv. Funct. Mater.* **2021**, *31*, 2103283.

[7] Z. Zheng, J. Wang, P. Bi, J. Ren,Y. Wang, Y. Yang, X. Liu,S. Zhang, J. Hou, *Joule* **2022**, *6*, 1.

[8] Q. Fan, W. Su, S. Chen, W. Kim, X. Chen, B. Lee, T. Liu, U. A. Méndez-Romero, R. Ma, T. Yang, W. Zhuang, Y. Li, Y. Li, T.-S. Kim, L. Hou, C. Yang, H. Yan, D. Yu, E. Wang, *Joule* **2020**, *4*, 658.

[9] J.-W. Lee, C. Sun, B. S. Ma, H. J. Kim, C. Wang, J. M. Ryu, C. Lim, T.-S. Kim, Y.-H. Kim, S.-K. Kwon, B. J. Kim, *Adv. Energy Mater.* **2021**, *11*, 2003367.

[10] G. Wang, F. S. Melkonyan, A. Facchetti, T. J. Marks, *Angew. Chem. Int. Ed.* **2019**, *58*, 4129.

[11] Y. Qin, N. Balar, Z. Peng, A. Gadisa, I. Angunawela, A. Bagui, S. Kashani, J. Hou, H. Ade, *Joule* **2021**, *5*, 2129.

[12] H. Yu, M. Pan, R. Sun, I. Agunawela, J. Zhang, Y. Li, Z. Qi, H. Han, X. Zou, W. Zhou, S. Chen, J. Y. L. Lai, S. Luo, Z. Luo, D. Zhao, X. Lu, H. Ade, F. Huang, J. Min, H. Yan, *Angew. Chem. Int. Ed.* **2021**, *60*, 10137.

[13] Q. Fan, H. Fu, Q. Wu, Z. Wu, F. Lin, Z. Zhu, J. Min, H. Y. Woo, A. K.-Y. Jen, *Angew. Chem. Int. Ed.* **2021**, *60*, 15935.

[14] H. Fu, Y. Li, J. Yu, Z. Wu, Q. Fan, F. Lin, H. Y. Woo, F. Gao, Z. Zhu, A. K. Y. Jen, *J. Am. Chem. Soc.* **2021**, *143*, 2665.

[15] J. Yang, B. Xiao, A. Tang, J. Li, X. Wang, E. Zhou, *Adv. Mater.* **2019**, *31*, 1804699.

[16] X. Zhan, Z. a. Tan, B. Domercq, Z. An, X. Zhang, S. Barlow, Y. Li, D. Zhu, B. Kippelen, S. R. Marder, *J. Am. Chem. Soc.* **2007**, *129*, 7246.

[17] Z. Li, X. Xu, W. Zhang, X. Meng, W. Ma, A. Yartsev, O. Inganäs, M. R. Andersson, R. A. J. Janssen, E. Wang, *J. Am. Chem. Soc.* **2016**, *138*, 10935.

[18] R. Zhao, N. Wang, Y. Yu, J. Liu, *Chem. Mater.* **2020**, *32*, 1308.

[19] L. Gao, Z.-G. Zhang, L. Xue, J. Min, J. Zhang, Z. Wei, Y. Li, *Adv. Mater.* **2016**, *28*, 1884.

[20] J. Yuan, Y. Xu, G. Shi, X. Ling, L. Ying, F. Huang, T. H. Lee, H. Y. Woo, J. Y. Kim, Y. Cao, W. Ma, *J. Mater. Chem. A* **2018**, *6*, 10421.

[21] S. Shi, P. Chen, Y. Chen, K. Feng, B. Liu, J. Chen, Q. Liao, B. Tu, J. Luo, M. Su, H. Guo, M.-G. Kim, A. Facchetti, X. Guo, *Adv. Mater.* **2019**, *31*, 1905161.

[22] Z.-G. Zhang, Y. Yang, J. Yao, L. Xue, S. Chen, X. Li, W. Morrison, C. Yang, Y. Li, *Angew. Chem. Int. Ed.* **2017**, *56*, 13503.

[23] N. Su, R. Ma, G. Li, T. Liu, L.-W. Feng, C. Lin, J. Chen, J. Song, Y. Xiao, J. Qu, X. Lu, V. K. Sangwan, M. C. Hersam, H. Yan, A. Facchetti, T. J. Marks, *ACS Energy Lett.* **2021**, *6*, 728.

[24] T. Wang, R. Sun, W. Wang, H. Li, Y. Wu, J. Min, *Chem. Mater.* **2021**, *33*, 761.

[25] H. Yao, L.-K. Ma, H. Yu, J. Yu, P. C. Y. Chow, W. Xue, X. Zou, Y. Chen, J. Liang, L. Arunagiri, F. Gao, H. Sun, G. Zhang, W. Ma, H. Yan, *Adv. Energy Mater.* **2020**, *10*, 2001408.

[26] Q. Fan, R. Ma, T. Liu, W. Su, W. Peng, M. Zhang, Z. Wang, X. Wen, Z. Cong, Z. Luo, L. Hou, F. Liu, W. Zhu, D. Yu, H. Yan, E. Wang, *Sol. RRL* **2020**, *4*, 2000142.

[27] C. Wang, F. Moro, S. Ni, Q. Zhang, G. Pan, J. Yang, F. Zhang, I. A. Buyanova, W. M. Chen, X. Liu, M. Fahlman, *Nano Energy* **2020**, *72*, 104677.

[28] K. Feng, J. Huang, X. Zhang, Z. Wu, S. Shi, L. Thomsen, Y. Tian, H. Y. Woo, C. R. McNeill, X. Guo, *Adv. Mater.* **2020**, *32*, 2070226.

[29] T. Liu, T. Yang, R. Ma, L. Zhan, Z. Luo, G. Zhang, Y. Li, K. Gao, Y. Xiao, J. Yu, X. Zou, H. Sun, M. Zhang, T. A. Dela Peña, Z. Xing, H. Liu, X. Li, G. Li, J. Huang, C. Duan, K. S. Wong, X. Lu, X. Guo, F. Gao, H. Chen, F. Huang, Y. Li, Y. Li, Y. Cao, B. Tang, H. Yan, *Joule* **2021**, *5*, 914.

[30] Z.-G. Zhang, Y. Li, *Angew. Chem. Int. Ed.* **2021**, *60*, 4422.

[31] Q. Fan, Q. An, Y. Lin, Y. Xia, Q. Li, M. Zhang, W. Su, W. Peng, C. Zhang, F. Liu, L. Hou, W. Zhu, D. Yu, M. Xiao, E. Moons, F. Zhang, T. D. Anthopoulos, O. Inganäs, E. Wang, *Energy Environ. Sci.* **2020**, *13*, 5017.

[32] Q. Fan, R. Ma, T. Liu, J. Yu, Y. Xiao, W. Su, G. Cai, Y. Li, W. Peng, T. Guo, Z. Luo, H. Sun, L. Hou, W. Zhu, X. Lu, F. Gao, E. Moons, D. Yu, H. Yan, E. Wang, *Sci. China Chem.* **2021**, *64*, 1380.

[33] J. Du, K. Hu, L. Meng, I. Angunawela, J. Zhang, S. Qin, A. Liebman-Pelaez, C. Zhu, Z. Zhang, H. Ade, Y. Li, *Angew. Chem. Int. Ed.* **2020**, *59*, 15181.

[34] Y. Wang, N. Wang, Q. Yang, J. Zhang, J. Liu, L. Wang, *J. Mater. Chem. A* **2021**, *9*, 21071.

[35] H. Wang, H. Chen, W. Xie, H. Lai, T. Zhao, Y. Zhu, L. Chen, C. Ke, N. Zheng, F. He, *Adv. Funct. Mater.* **2021**, *31*, 2100877.

[36] T. Jia, J. Zhang, W. Zhong, Y. Liang, K. Zhang, S. Dong, L. Ying, F. Liu, X. Wang, F. Huang, Y. Cao, *Nano Energy* **2020**, *72*, 104718.

[37] Z. Luo, T. Liu, R. Ma, Y. Xiao, L. Zhan, G. Zhang, H. Sun, F. Ni, G. Chai, J. Wang, C. Zhong, Y. Zou, X. Guo, X. Lu, H. Chen, H. Yan, C. Yang, *Adv. Mater.* **2020**, *32*, e2005942.

[38] H. Sun, H. Yu, Y. Shi, J. Yu, Z. Peng, X. Zhang, B. Liu, J. Wang, R. Singh, J. Lee, Y. Li, Z. Wei, Q. Liao, Z. Kan, L. Ye, H. Yan, F. Gao, X. Guo, *Adv. Mater.* **2020**, *32*, 2004183.

[39] R. Sun, W. Wang, H. Yu, Z. Chen, X. Xia, H. Shen, J. Guo, M. Shi, Y. Zheng, Y. Wu, W. Yang, T. Wang, Q. Wu, Y. Yang, X. Lu, J. Xia, C. J. Brabec, H. Yan, Y. Li, J. Min, *Joule* **2021**, *5*, 1548.

[40] J. Wu, Y. Meng, X. Guo, L. Zhu, F. Liu, M. Zhang, *J. Mater. Chem. A* **2019**, *7*, 16190.

[41] C. Li, J. Zhou, J. Song, J. Xu, H. Zhang, X. Zhang, J. Guo, L. Zhu, D. Wei, G. Han, J. Min, Y. Zhang, Z. Xie, Y. Yi, H. Yan, F. Gao, F. Liu, Y. Sun, *Nat. Energy* **2021**, *6*, 605.

[42] L. Zhu, M. Zhang, G. Zhou, T. Hao, J. Xu, J. Wang, C. Qiu, N. Prine, J. Ali, W. Feng, X. Gu, Z. Ma, Z. Tang, H. Zhu, L. Ying, Y. Zhang, F. Liu, *Adv. Energy Mater.* **2020**, *10*, 1904234.

[43] L. J. A. Koster, V. D. Mihailetchi, H. Xie, P. W. M. Blom, *Appl. Phys. Lett.* **2005**, *87*, 203502.

[44] P. W. M. Blom, V. D. Mihailetchi, L. J. A. Koster, D. E. Markov, *Adv. Mater.* **2007**, *19*, 1551.

[45] T. Xia, Y. Cai, H. Fu, Y. Sun, *Sci. China Chem.* **2019**, *62*, 662.

[46] T. Liu, L. Huo, S. Chandrabose, K. Chen, G. Han, F. Qi, X. Meng, D. Xie, W. Ma, Y. Yi, J. M. Hodgkiss, F. Liu, J. Wang, C. Yang, Y. Sun, *Adv. Mater.* **2018**, *30*, 1707353.

[47] J. Comyn, *Int. J. Adhes. Adhes.* **1992**, *12*, 145.

[48] S. Nilsson, A. Bernasik, A. Budkowski, E. Moons, *Macromolecules* **2007**, *40*, 8291.

[49] W. Shockley, H.J. Queisser, *J. Appl. Phys.* **1961**, *32*, 510.

[50] U. Rau, *Phy. Rev. B* **2007**, *76*, 8.

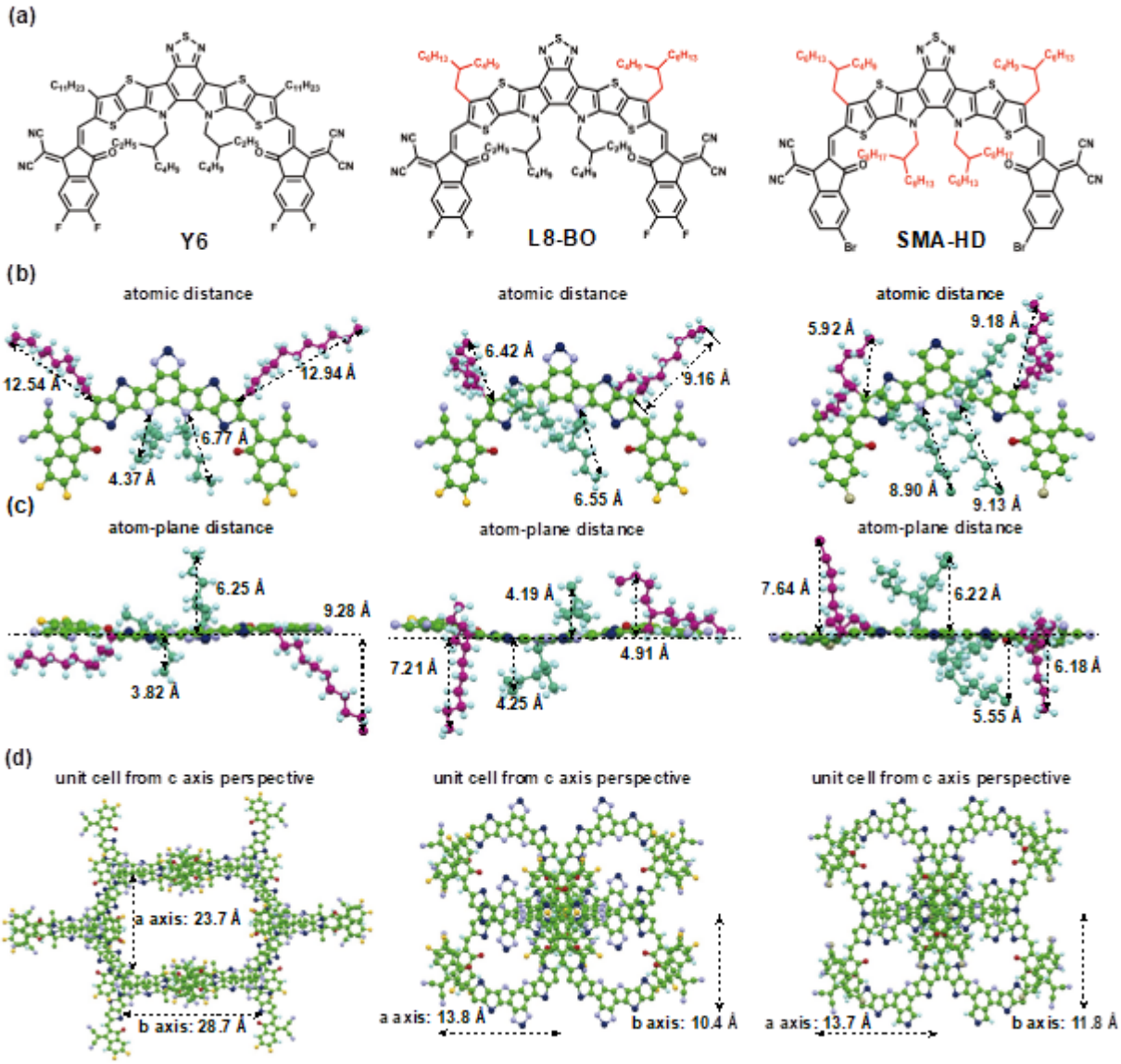

Figure 1. (a) Molecular structures of Y6, L8-BO and SMA-HD. (b) The main view and (c) side view of a molecular conformation sketch of Y6, L8-BO and SMA-HD according to the single-crystal data. The dashed lines represent the side-chain self-assembly distance of SMAs. (d) The main view of a molecular packing sketch of Y6, L8-BO and SMA-HD. For L8-BO and SMA-HD, the horizontal and the vertical values represent half of the a and b axes parameters of unit cell, respectively. For Y6, the horizontal and vertical values represent the a axis and half of the b axis parameters of the unit cell.

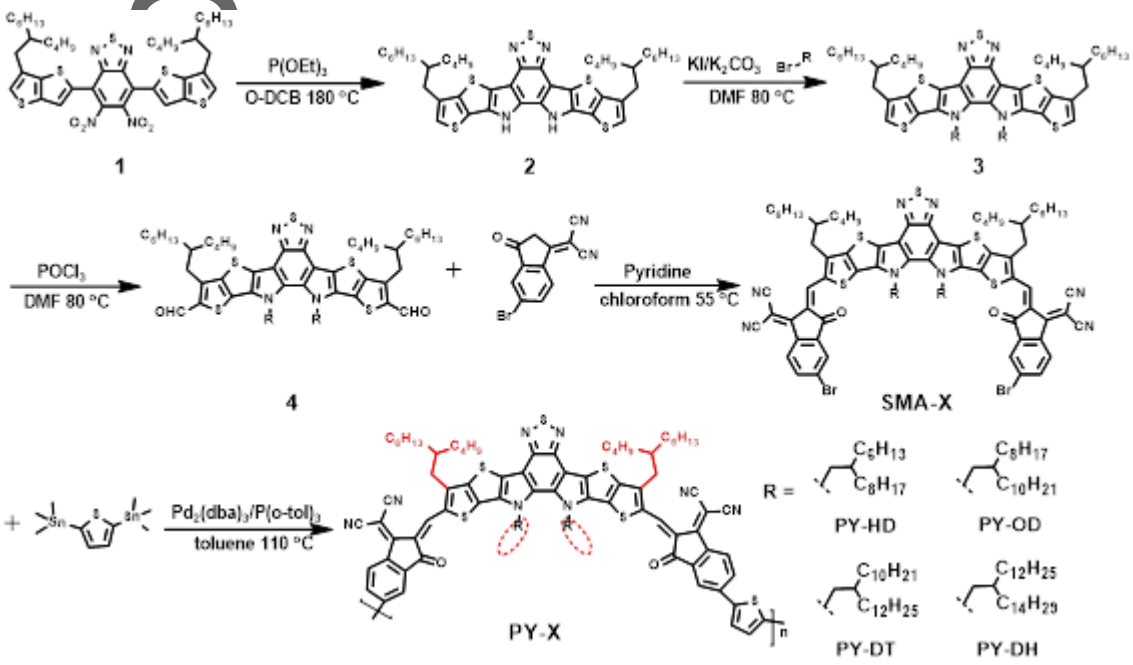

Scheme 1. Synthetic routes for PY-X acceptors with different branched side chains.

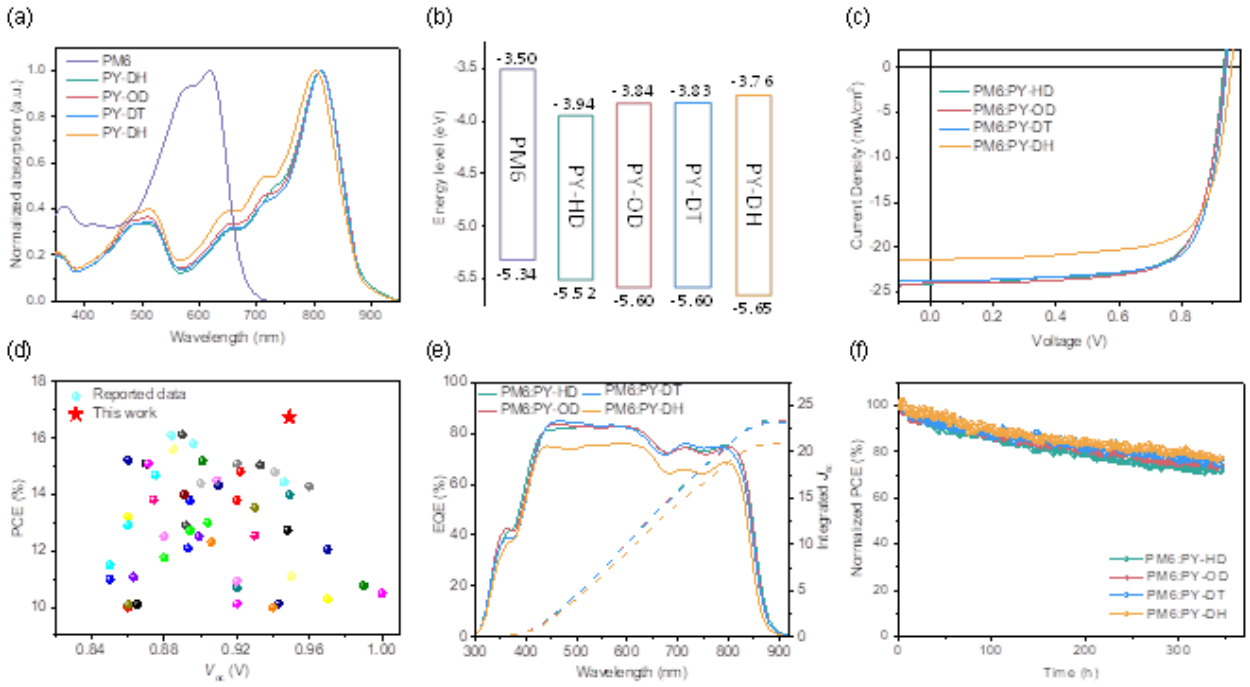

Figure 2. (a) Normalized absorption spectra of PM6 and PY-X films. (b) Energy level diagrams of PM6 and PY-X. (c) *J-V* characteristics for the optimized binary all-PSCs. (d) Comparison of our work with reported PCE and V_{oc} values for binary all-PSCs with PCEs over 10% in the literature. (e) EQE spectra (solide lines) and integrated current densities (dashed lines) of the optimized binary all-PSCs. (f) Photostability of the all-PSCs devices measured under continuous 1 sun illumination in air.

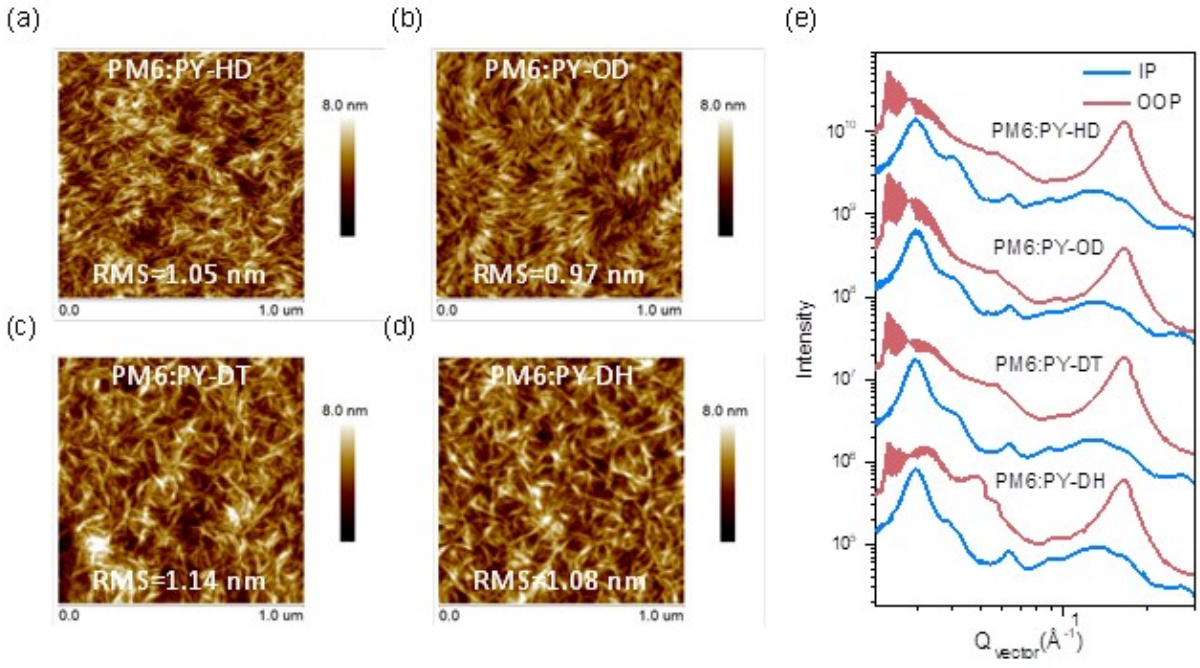

Figure 3. AFM height images of the optimized PM6:PY-HD (a), PM6:PY-OD (b), PM6:PY-DT (c), and PM6:PY-DH (d) films. (e) The in-plane and out-of-plane line-cut profiles extracted from the 2D GIWAXS of PM6:PY-HD, PM6:PY-OD, PM6:PY-DT, and PM6:PY-DH films, respectively.

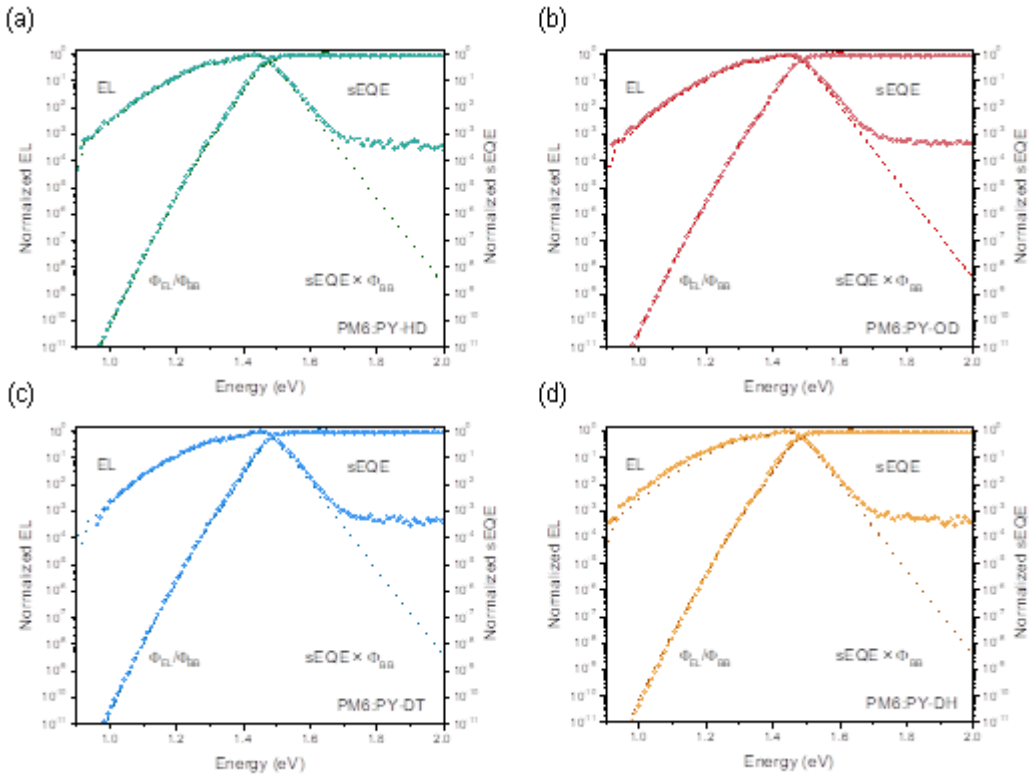

Figure 4. Normalized EL and normalized sEQE of reciprocally calculated EL and EQE (dashed lines) as a function of energy for all-PSCs based on PM6:PY-HD (a), PM6:PY-OD (b), PM6:PY-DT (c), and PM6:PY-DH (d). The ratio of ϕ_{EL} and ϕ_{BB} is used to calculate the EQE and the product of sEQE and ϕ_{BB} is used to calculate the EL, where ϕ_{EL} and ϕ_{BB} represent the emitted photon flux and the room-temperature black body photon flux, respectively.

Table 1. Summary of device parameters of the optimized all-PSCs.

Active layer	V_{oc} (V)	J_{sc} (mA cm^{-2})	FF (%)	PCE[a)] (%)
PM6:BY-HD	0.937	24.05	72.8	16.41
PM6:BY-OD	0.942	23.05	72.2	16.52
PM6:BY-DT	0.949	22.72	74.4	16.76
PM6:BY-DH	0.961	21.20	72.2	14.86

[a)]The average parameters were calculated from 20 devices.

[b)]The certified result by National Institute of Metrology (NIM), China

Table 2. Total V_{loss} and different contributions to V_{loss} in the binary all-PSCs.

Active layer	V_{oc} [V]	E_g[a)] [eV]	V_{loss} [eV]	V_{oc}^{SQ}[b)] [V]	V_{oc}^{rad}[c)] [V]	ΔE_1 [eV]	ΔE_2 [eV]	ΔE_3[d)] [eV]	EQE_{EL}

PM6:PY-HD	0.94	1.48	0.55	1.21	1.12	0.27	0.09	0.19	5.43×10^{-4}
PM6:PY-OD	0.95	1.49	0.55	1.22	1.13	0.27	0.09	0.18	6.85×10^{-4}
PM6:PY-DT	0.95	1.49	0.54	1.22	1.13	0.27	0.09	0.18	7.15×10^{-4}
PM6:PY-DH	0.96	1.49	0.53	1.22	1.14	0.27	0.08	0.18	8.32×10^{-4}

[a)] E_g is the optical bandgap of the film determined from the normalized reduced absorption and PL spectra.

[b)] V_{oc}^{SQ} is the maximum V_{oc} by the SQ limit.

[c)] V_{oc}^{rad} is the voltage loss associated with radiative recombination.

[d)] ΔE_3 is the voltage loss associated with non-radiative recombination.

Table of Contents:

A series of polymer acceptors named PY-X have been synthesized. By optimizing the length of branched alkyl chains, PY-HD (2-hexyldecyl substitution)-based all polymer solar cell delivers a high efficiency of 16.76%, with an open-circuit voltage of 0.949 V, and an extremely low non-rad non-radiative voltage loss of 0.18 V, representing the highest efficiency for binary all polymer solar cells.

Keywords: All polymer solar cell, polymer acceptor, small molecular acceptor, branched side chain, efficiency

Yun Li, Jiali Song, Yicai Dong, Hui Jin, Jingming Xin, Shijie Wang, Yunhao Cai,* Lang Jiang, Wei Ma, Zheng Tang, and Yanming Sun*

Polymerized Small Molecular Acceptor with Branched Side Chains for All Polymer Solar Cells with Efficiency over 16.7%

ToC Figure